Journal of Power Sources 331 (2016) 553–565

Contents lists available at ScienceDirect

Journal of Power Sources

journal homepage: www.elsevier.com/locate/jpowsour

An optimal control strategy for standalone PV system with Battery-Supercapacitor Hybrid Energy Storage System

Lee Wai Chong*, Yee Wan Wong, Rajprasad Kumar Rajkumar, Dino Isa

Department of Electrical and Electronic Engineering, The University of Nottingham Malaysia Campus, Jalan Broga, Semenyih 43500, Selangor, Malaysia

HIGHLIGHTS

- The proposed control strategy comprises low pass filter and fuzzy logic controller.
- Membership functions of fuzzy logic controller are optimized by PSO.
- The dynamic stress and peak current of the battery are greatly reduced.
- The level of utilization of supercapacitor are significantly increased.

ARTICLE INFO

Article history:
Received 6 June 2016
Received in revised form
16 August 2016
Accepted 12 September 2016

Keywords:
Control strategy
Hybrid Energy Storage System
Fuzzy logic controller
Battery
Supercapacitor
Particle swarm optimization

ABSTRACT

This paper proposes an optimal control strategy for a standalone PV system with Battery-Supercapacitor Hybrid Energy Storage System to prolong battery lifespan by reducing the dynamic stress and peak current demand of the battery. Unlike the conventional methods which only use either filtration based controller (FBC) or fuzzy logic controller (FLC), the proposed control strategy comprises of a low-pass filter (LPF) and FLC. Firstly, LPF removes the high dynamic components from the battery demand. FLC minimizes the battery peak current demand while constantly considering the state-of-charge of the supercapacitor. Particle swarm optimization (PSO) algorithm optimizes the membership functions of the FLC to achieve optimal battery peak current reduction. The proposed system is compared to the conventional system with battery-only storage and the systems with conventional control strategies (Rule Based Controller and FBC). The proposed system reduces the battery peak current, battery peak power, maximum absolute value of the rate of change of power and average absolute value of the rate of change of power by 16.05%, 15.19%, 77.01%, and 95.59%, respectively as compared to the conventional system with battery-only storage. Moreover, he proposed system increases the level of supercapacitor utilization up to 687.122% in comparison to the conventional control strategies.

1. Introduction

Batteries are commonly implemented in standalone PV power systems to fulfill the power mismatch between the PV power generation and the load demand. Generally, a battery would encounter frequent deep cycles and irregular charging pattern due to the varying output of PV and the intermittent high power demand of the load. These operations would shorten the battery lifespan and increase the replacement cost of the battery [1–3]. Battery-Supercapacitor Hybrid Energy Storage System (HESS) is thus a practical solution to minimize the battery stress, battery size and the total capital cost of the system [4]. The technical characteristics of battery and supercapacitor (SC), such as specific power, specific energy, response time and durability, are complementary.

A control strategy is essential for the HESS to optimize the energy utilization and energy sustainability to a maximum extent as it is the algorithm which manages the power flow of the battery and SC. One of the common aims of HESS implementation is to prolong the battery lifespan by reducing the peak current demand and the dynamic stress of the battery. Battery peak current reduction would reduce the internal voltage drop in the battery and improve the battery efficiency [4,5]. Reduction in battery dynamic stress minimizes the heating and the internal losses of the battery [5,6].

Table 1 summarizes that Rule Based Controller (RBC) [7–12] and Filtration Based Controller (FBC) [13–18] that are commonly

* Corresponding author.
E-mail addresses: kecx5cla@nottingham.edu.my, leewaichong@outlook.com (L.W. Chong).

http://dx.doi.org/10.1016/j.jpowsour.2016.09.061
0378-7753/

Nomenclature

$\|Ah\|_{SC}$	Absolute value of accumulated ampere hours of supercapacitor (Ah)
$\|\Delta P\|$	Absolute value of the rate of change of power (W s^{-1})
$\|\Delta P\|max$	Maximum $\|\Delta P\|$ (W s^{-1})
$\|\Delta P\|mean$	Mean $\|\Delta P\|$ (W s^{-1})
Δt	Time Step (s)
ANN	Artificial Neural Network
dP	Power Deficit between P_{PV} and P_{load} (W)
f(x)	Fitness Function
FBC	Filtration Based Controller
FLC	Fuzzy Logic Controller
GA	Genetic Algorithm
Gbest	Global Best Value
H	High
HESS	Hybrid Energy Storage System
HPF	High Pass Filter
HSS	Hydrogen Storage System
ib1	Battery Current Threshold 1
ib2	Battery Current Threshold 2
I_{batt}	Battery Current (A)
I_{batt_peak}	Battery Peak Current Demand (A)
i_L	Inductor Current (A)
K1	Gradient 1
K2	Gradient 2
L	Low
LPF	Low Pass Filter
M	Medium
MF	Membership Function
mf	Number of Membership Functions
n	Number of Input Variables
NH	Negative High
NL	Negative Low
P(t)	Power at time t (W)
P(t-Δt)	Power at time t−Δt (W)
P_{batt}	Battery Power (W)
pbest	Personal Best Value
PH	Positive High
P_H	Peak Power Demand (W)
P_{HF}	High Frequency Power Demand (W)
PL	Positive Low (W)
P_{LF}	Low Frequency Power Demand (W)
P_{load}	Load Demand (W)
P_{PV}	PV Output Power (W)
P_{sc}	Supercapacitor Power (W)
Psc^*	Supercapacitor Reference Power (W)
P_{sc}'	Converted Supercapacitor Power (W)
PSO	Particle Swarm Optimization
P_{batt_peak}	Battery Peak Power Demand (W)
RBC	Rule Based Controller
REPS	Renewable Energy Power System
SC	Supercapacitor
SOC	State-of-Charge (%)
SOC_{batt}	State-of-Charge of Battery (%)
$SOC_{batt\_average}$	Average State-of-Charge of Battery (%)
SOC_{batt_final}	Final State-of-Charge of Battery (%)
SOCsc	State-of-Charge of Supercapacitor (%)
SVM	Support Vector Machine
WCA	Water Cycle Algorithm
Z	Zero
α	Power Sharing Ratio
η_{dcdc}	Efficiency of Bidirectional DC-DC Converter (%)

Table 1
Summary of literature [7–18] showing analysis on the type of RE sources, and control strategy for system with Battery-Supercapacitor HESS only.

Ref.	RE source(s)	HESS	Control strategy	Optimization
[7]	PV	Battery/SC	RBC	–
[8]	PV	Battery/SC	RBC	–
[9]	Wind	Battery/SC	RBC	–
[10]	PV	Battery/SC	RBC	–
[11]	PV	Battery/SC	RBC	–
[12]	PV	Battery/SC	RBC	–
[13]	Wind & PV	Battery/SC	FBC & ANN	–
[14]	Wind	Battery/SC	FBC	–
[15]	Wind	Battery/SC	FBC	–
[16]	PV	Battery/SC	FBC	–
[17]	Wind	Battery/SC	FBC	–
[18]	PV	Battery/SC	FBC	–
This Study	PV	Battery/SC	FBC & FLC	PSO

employed in renewable energy power system (REPS) with Battery-Supercapacitor HESS. Despite RBC being simple to implement, it is rigid and incapable of adapting to real-time system condition as it has pre-defined thresholds, rules and operations [30]. In Refs. [9] and [27], both studies implemented RBC for off-grid REPS with HESS. In these studies, the output power of the renewable energy sources is free of fluctuation with the utilization of filtered wind speed and solar irradiation profiles. This is not realistic as the output power of renewable energy sources would fluctuate in real life due to the varying weather condition.

FBC decomposes the power demand into high and low frequency components by utilizing a filter and it is excellent in smoothening the battery current. In Ref. [16], the authors implemented a low pass filter (LPF) based FBC to reduce the charge/discharge rate of the battery. However, the SOC of the energy storage systems was considered as trivial in the control strategy. In fact, FBC is not effective in minimizing the peak power demand of the battery as it can only process the frequency of the power demand.

Table 2 shows that fuzzy logic controller (FLC) is commonly employed in REPS with hydrogen storage system (HSS)-battery HESS. However, there has been little discussion about the

Table 2
Summary of literature [19–29] showing analysis on the type of RE sources, and control strategy for system with HESS.

Ref.	RE source(s)	HESS	Control strategy	Optimization
[19]	Wind	Battery/HSS	RBC	–
[20]	Wind & PV	Battery/HSS	Neuro-fuzzy	Neuro-fuzzy
[21]	Wind & PV	Battery/HSS	RBC & FLC	–
[22]	Wind	Battery/SMES	FLC	GA
[23]	Wind & PV	Battery/HSS	FLC	WCA
[24]	Wind & PV	Battery/HSS	ANN	–
[25]	Wind	Battery/HSS	FLC	PSO & SFL
[26]	Wind & PV	Battery/HSS	FLC	PSO
[27]	Wind & PV	Battery/HSS	RBC	–
[28]	PV	Battery/HSS	RBC	–
[29]	Wind & PV	Battery/HSS	RBC	–
This Study	PV	Battery/SC	FBC & FLC	PSO

implementation of FLC in REPS with Battery-Supercapacitor HESS. FLC is easily understandable and it is insensitive to variations of the parameters. Besides, it does not require an exact model of the system and training process. In Ref. [31], the authors highlighted that FLC could achieve better performance compared to RBC and FBC. Moreover, the FLC reduces more than 50% of the battery capacity loss in comparison to battery-only configuration [31]. However, the membership functions (MFs) of the FLC in Ref. [31] are not optimized and do not guarantee the optimal performance. The MFs of FLC are usually determined by using trial-and-error method which is time-consuming and lacks optimization [32,33].

The prediction of solar irradiance [34–36] and electrical load [37–39] are possible by using of machine learning algorithms particularly artificial neural network (ANN) and support vector machine (SVM). Hence, evolutionary algorithm such as Particle Swarm Optimization (PSO), Genetic Algorithm (GA) and other algorithms can be implemented to optimize the MFs of FLC with the aim to solve the multi-objective optimization problems. In Ref. [23], the authors optimized the Mandami-type FLC for PV/wind with HSS-Battery HESS by using Water Cycle Algorithm (WCA) correlating to the objectives of LPSP and O&M cost minimization [23]. In a study, the authors presented a list of literature showing the lack of optimized FLC for power flow regulation and energy management of REPS [40]. Similarly, Tables 1 and 2 shows limited research on the optimization of control strategy for REPS with Battery-Supercapacitor HESS.

This paper proposes an optimal control stratergy for standalone PV power system with Battery-Supercapacitor HESS. The objectives of the proposed control strategy are to reduce the dynamic stress and the peak current demand of the battery while constantly considering the SOC level of the SC (SOCsc). The proposed control strategy comprises of a LPF and a Sugeno-type FLC. As the fluctuations of PV output has been taken into account in this study, the LPF filtration process is executed to allocate the high dynamic component of the power demand to the SC and refer the low dynamic component of the power demand to the FLC. The Sugeno-type FLC is computationally efficient and it works well with optimization and adaptive techniques [41]. Therefore, it is utilized to reduce the peak current demand of the battery by manipulating the amount of power to be charged/discharged by the SC based on the real-time power demand and SOCsc. PSO is applied to determine the optimal MFs of FLC in order to minimize the battery peak current. The performance of the proposed system is compared to the conventional systems (standalone PV system with battery storage, standalone PV system with batter-supercapacitor HESS with RBC, and standalone PV system with batter-supercapacitor HESS with FBC) by Simulink with the setup of rural household load profile and the actual solar irradiation profile of a rainy day. Moreover, two additional actual solar irradiation profiles are modelled and tested with the proposed model to evaluate the system performance in different scenarios.

This paper is organized as follows: Section 2 demonstrates the Simulink models of the proposed system while Section 3 explains the structure of the conventional control strategies (RBC and FBC) and the proposed control strategy in detail. Section 4 presents the results and discussions of the PSO optimization and the comparison between the conventional systems and the proposed system. Finally, a succinct conclusion has been drawn in Section 5.

2. System structure and modelling

2.1. Standalone PV system with Battery-Supercapacitor HESS

Fig. 1(a) illustrates the Simulink model of the standalone PV system with Battery-Supercapacitor HESS where the HESS of the proposed system is equipped with battery bank, SC, bidirectional DC-DC converter and control circuitry. The structure and detail of PV Array, Battery and Supercapacitor model are available in the Simulink library. Typically, the HESS takes the advantages of high energy density storage and high power density storage to achieve the desirable performance in which the Battery-Supercapacitor HESS is proposed in this work. However, a complex conditioning circuitry is required to combine the battery and supercapacitor as a single power source. As the SC voltage highly fluctuates due to its low energy density, the Battery-Supercapacitor HESS of the proposed system is implemented in a semi-active topology where a bidirectional DC-DC converter is placed next to the SC to decouple the SC with system. Fig. 1(b) depicts the structure of Semi-Active Battery-Supercapacitor HESS where a power electronic unit is employed to control the power flow of the SC based on the control strategy. The power electronic unit consists of a bidirectional DC-DC converter and a control circuitry. This topology allows for a sufficient degree of freedom to implement different control strategies [39]. In addition, this topology provides a good trade-off between the performance and the circuit complexity as only one DC-DC converter is employed.

In order to appropriately interface the batteries and the supercapacitors in the HESS, a bidirectional DC-DC converter is required to control the power flow in two directions. In this study, half-bridge bidirectional DC-DC converter, as illustrated in Fig. 1(c), is proposed to interface the batteries and SC. The half-bridge bidirectional DC-DC converter is capable of operating in buck mode and boost mode. It consists of two bi-positional switches realized using the transistors S1/S2 and diodes D1/D2 in a half bridge configuration. The high voltage side and low voltage side of the bidirectional DC-DC converter are connected to the DC bus and the SC respectively to allow for a flexible SC operation. The power is transferred from high voltage side to low voltage side (inductor current, $i_L > 0$) when the converter operates in buck mode. Similarly, the power is transferred from low voltage side to high voltage side ($i_L < 0$) when the converter operates in boost mode. Based on Fig. 1(a), the dynamic power balance of the proposed system can be expressed as below:

$$P_{PV} + P_{batt} + P'_{SC} - P_{load} = 0 \tag{1}$$

where P_{PV} is the power generation of the PV, P_{batt} is the power flow of the battery, P_{load} is the power demand of the load, and $P_{sc}'$is the power flow of SC power after the power conversion by the DC-DC converter. In actual operation, the efficiency of the DC-DC converter is less than 100%. Therefore, the power transfer from SC to DC bus can be expressed as equation (2).

$$P'_{SC} = \eta_{DCDC} \times P_{SC} \tag{2}$$

where P_{SC} is the power flow of SC and η_{dcdc} is the efficiency of the DC-DC converter. In this study, the efficiency of the DC-DC converter is assumed as 100%. Thus, the total power to be satisfied by the Battery-Supercapacitor HESS, dP, which is the power deficit between the P_{PV} and P_{load}, is defined in equation (3).

$$dP = P_{PV} - P_{load} = P_{batt} + P_{SC} \tag{3}$$

The specification of the proposed system is listed in Table 3.

In order to evaluate the system performance, the actual solar irradiation profile of a rainy day in The University of Nottingham Malaysia Campus on 29th December 2014, as shown in Fig. 2(a), is modelled to ensure a low level PV power generation. As a result, the stress level of the HESS is increased. Besides, Fig. 2(b) illustrates the rural household load profile which is extracted from Ref. [41] and modified to impose more stress to the HESS. The high power

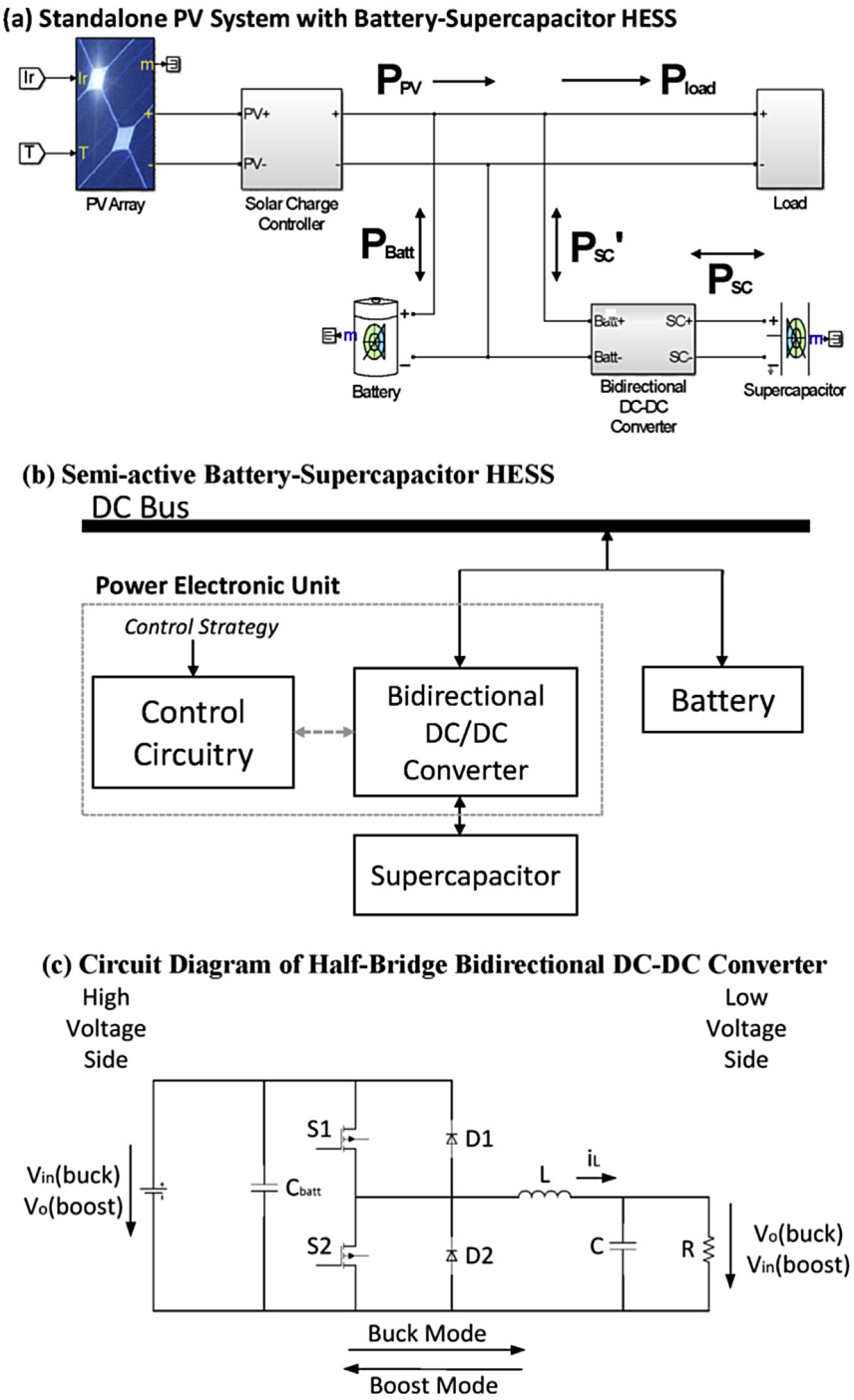

Fig. 1. Models of the system. (a) Simulink model of Standalone PV System with Battery-Supercapacitor HESS. (b) Block Diagram of Semi-Active Battery-Supercapacitor HESS. (c) Circuit Diagram of Half-Bridge Bidirectional DC-DC Converter.

Table 3
The Specification of the Standalone PV System with Battery-Supercapacitor HESS.

Component	Rating	
PV	Power	1.2 kW
Battery	Type	Lead-acid
	Voltage	48 V
	Capacity	300 Ah
Supercapacitor	Voltage	45 V
	Capacitance	500 F

demand of the load occurred during the day time from 13:00 to 17:00 with the average power demand of 357 W. The peak load demand of day is 370 W at 14:00. Fig. 2(c) demonstrates the power generation of PV based on the solar irradiation profile in Fig. 2(a). By referring to equation (3), the power demand of the HESS, which is the power deficit between PV output power and the load demand, is illustrated in Fig. 2(d).

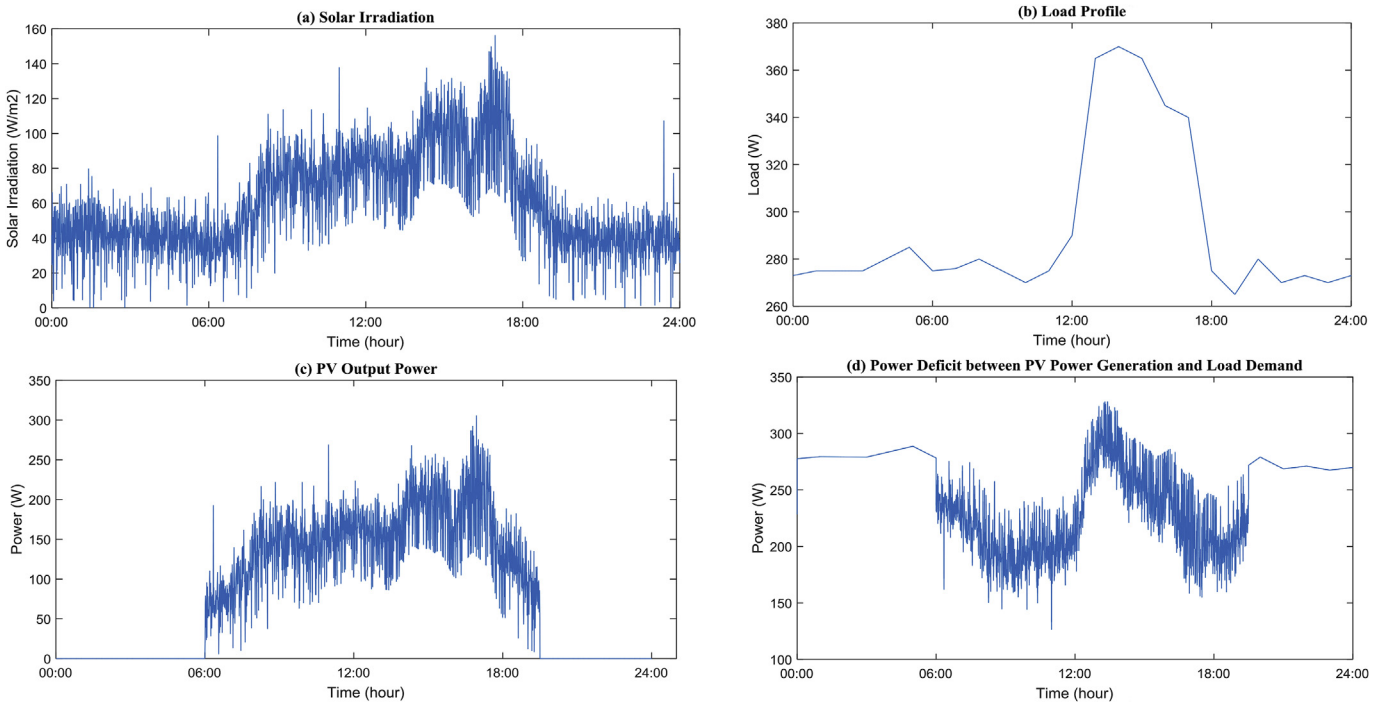

Fig. 2. Simulation Profiles: (a) Solar Irradiation Profile on 29th Dec 2014 (b) Daily Load Profile of a Rural Household (c) PV Power Generation based on the Solar Irradiation Profile on 29th Dec 2014 (d) Power Mismatch between PV Output Power and Load Demand.

3. Control strategy

The control strategy manages the power flow of the HESS based on the real-time system conditions. It is usually complex and required to operate continuously in order to fulfill the multiple objectives. Optimal control of the HESS is crucial to optimize the energy utilization and sustainability to a maximum extent. The common aims of the control strategies are listed as following [7–28]:

i. To prevent the deep discharge of the battery.
ii. To reduce the peak power demand, charge/discharging cycle, and dynamic stress level of battery.
iii. To maintain a stable DC voltage.
iv. To reduce the loss of power supply possibility (LPSP) and the operational and maintenance (O&M) cost.
v. To improve the overall efficiency of the system.

Generally, the control strategies can be characterized as classical control strategies and intelligent control strategies. The classical control strategies such as Rule based controller (RBC) and Filtration based Controller (FBC) are simple and easy to be implemented as they do not require complicated processing [30]. However, they are normally sensitive to the parameter variation and rigid [42]. Intelligent control strategy such as Fuzzy Logic Controller (FLC) is more robust and efficient compared to classical control strategies as it enhances the dynamic behavior of the system without requiring an exact model of the system [42]. However, the MFs of FLC are usually determined by using the trial-and-error method which is time-consuming and lacking of optimization [26,43].

As summarized in Table 1, the conventional control strategies such as RBC and FBC are commonly implemented in REPS with Battery-Supercapacitor HESS. In this study, two simple conventional control strategies (RBC and FBC) are compared with the proposed control strategy. Fig. 3 illustrates the structures of the RBC, FBC, and the proposed strategy. The operating range of SOCsc of all the models with SC is limited within the range of 50%–100% in order to allow the utilization of 75% of the overall SC energy [44].

3.1. Rule based controller (RBC)

The RBC uses a set of rules to decide the power sharing between the battery and SC. It is simple to be implemented as it does not require complicated processing. However, RBC is very sensitive to the variation of parameter as it has pre-defined rules and operations [42]. A RBC, which is extracted from Ref. [45], is developed and expressed in the form of dead-zone function as shown in Fig. 3(a) ib1 and ib2 are the battery current thresholds and K1 and K2 are the slope gradients. When the battery current is within the thresholds ib1 and ib2, the battery would be the only source to meet the load demand. When the battery current demand exceeds the threshold ib1 or ib2, the excessive current demand will be shared among the battery and SC by the ratio of K1 or K2. The design, performance, and analysis of the control strategy are explained in detail in Ref. [45].

3.2. Filtration based controller (FBC)

The FBC uses a filter to decompose the dynamic components of the power demand into high-frequency components and low-frequency-components. This technique is simple and having less computational burden [16]. Fig. 3(b) illustrates the structure of high pass filter (HPF) based FBC which is extracted from Ref. [14]. The HPF characterizes the power demand in to high-frequency components (P_{HF}) and low-frequency components (P_{LF}) in which the P_{HF} and P_{LF} will be catered by SC and battery, respectively. The design, performance, and analysis of the control strategy are explained in detail in Ref. [14].

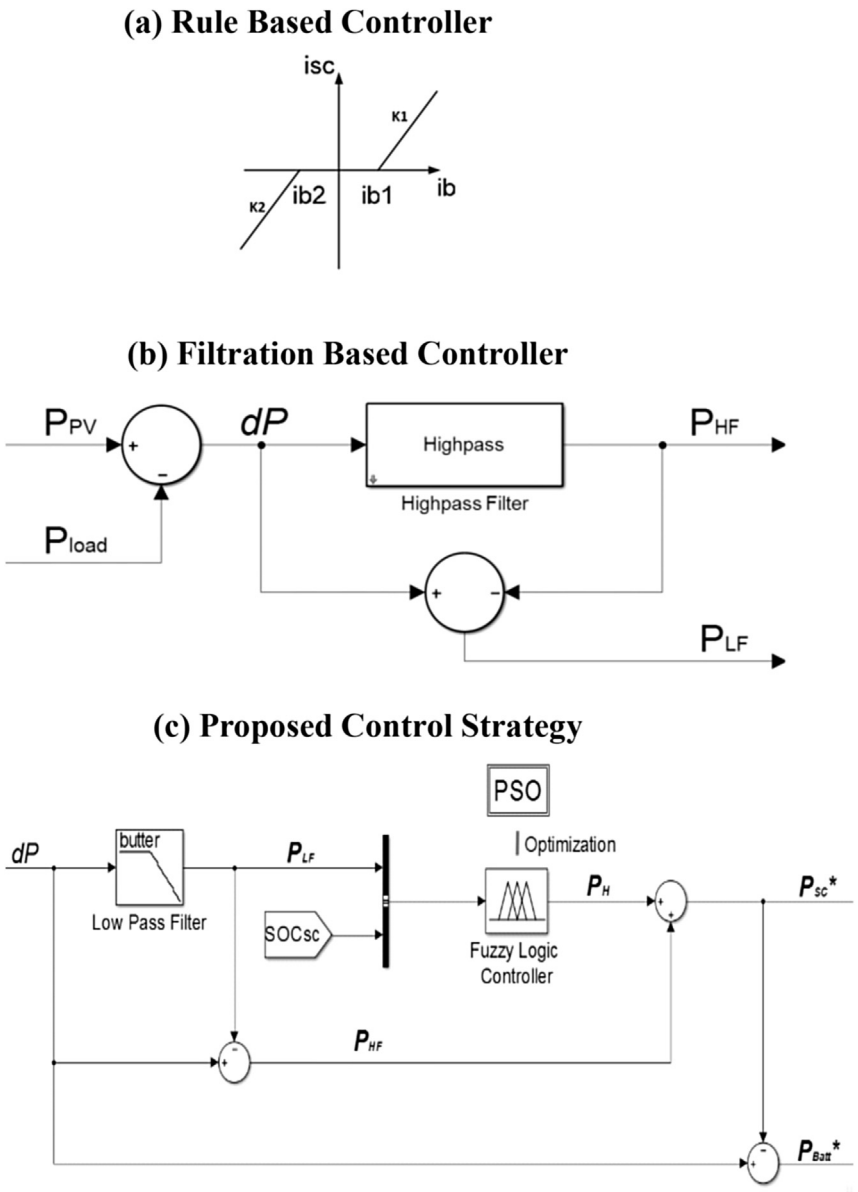

Fig. 3. Structures of the Control Strategies: (a) RBC in the form of deadzone function [45]. (b) FBC based on HPF [14]. (c) Proposed Control Strategy in this study.

3.3. Proposed control strategy

Fig. 3(c) illustrates the structure of the proposed control strategy which aims to minimize the dynamic stress and the peak current demand of the battery. The control strategy comprises of two parts that are the LPF and FLC. In order to achieve the optimal performance, PSO algorithm is implemented to optimize the membership functions (MFs) of the FLC. The structure of the proposed control strategy is explained in the following sections.

3.3.1. Low pass filter (LPF)

In actual operation, the power generation of PV and the load demand are highly fluctuating. In the conventional system, the battery is stressed to satisfy the highly fluctuating *dP*. The highly fluctuating battery current would produce an extensive heat inside the battery which leads to an increased battery internal resistance and lower efficiency [4,6]. Therefore, LPF is implemented to reduce the dynamic stress of the battery by decomposing the *dP* into P_{HF} and P_{LF}. The P_{LF} is the output of LPF while the P_{HF} is the difference between *dP* and P_{LF}.

$$P_{LF} = lowpassfilter(dP) \tag{4}$$

$$P_{HF} = dP - P_{LF} \tag{5}$$

The P_{HF} is a highly fluctuating power demand which is ideally to be absorbed by the SC while the P_{LF} is preferably to be met by the battery. This process would prevent the battery from supplying the high frequency components of *dP* and reduces the dynamic stress of the battery. After the LPF filtration, the P_{LF} is referred to the FLC for battery peak current reduction.

3.3.2. Fuzzy logic controller (FLC)

The purpose of FLC is to reduce the battery peak current while constantly considering the SOCsc. Sugeno type fuzzy system, is a computationally efficient system which works well with the optimization and adaptive techniques [41] and it is implemented in this

study. As shown in Fig. 3(c), the FLC has two inputs which are the P_{LF} and the SOCsc. The output of the FLC is the power sharing ratio, α, which is computed based on the real-time input variables. The MFs of the inputs are trapezoidal shapes. The MFs of the inputs and the output of the FLC are illustrated in Fig. 4.

The input variable P_{LF} has five MFs including positive high ("PH"), positive medium ("PM"), Low ("L"), negative low ("NL"), and negative high ("NH"). The positive P_{LF} is the power demand to be supplied by the HESS and the negative P_{LF} is the excessive power to be absorbed by the HESS. On the other hand, the input variable SOCsc has only three MFs namely High ("H"), Medium ("M"), and Low ("Low"). Meanwhile, the output variable α has five MFs that are PH, PL, zero ("Z"), NL, and NH. The positive and negative of membership functions indicate the power ratio to be supplied and absorbed by the SC, respectively.

The rules of the FLC are listed in Table 4. When the power demand of the P_{LF} is "L", the power sharing ratio, α, would be"Z" regardless of the SOCsc condition as the low power demand imposes little stress to the battery. When the P_{LF} is positive, α is set according to the level of the power demand and the SOCsc in order to reduce the peak current demand of the battery. When the P_{LF} is negative, α is set based on the excessive power and the SOCsc level to recover the charge of the SC. The power to be shared by the SC, P_H, can be calculated by using equation (6).

$$P_H = \alpha P_{LF} \tag{6}$$

The total power to be supplied by the SC, Psc^*, is the summation of P_{HF} and P_H.

Table 4
Fuzzy Logic Rules of FLC in this study.

		dP				
		PH	PL	L	NL	NH
SOCsc	H	PH	PL	Z	Z	Z
	M	PL	PL	Z	NL	NL
	L	Z	Z	Z	NL	NH

$$P_{SC}^* = P_{HF} + P_H \tag{7}$$

In the proposed system, the bidirectional DC-DC converter would regulate the power flow of SC according to Psc^*. As a result, the battery is expected to supply the power mismatch between Psc^* and dP as defined in equation (8).

$$P_{batt} = \mathrm{d}P - P_{SC}^* \tag{8}$$

3.3.3. Particle swarm optimization

The PSO algorithm is a population based optimization method inspired by social behavior of flocks of birds and fish looking for food [26]. PSO is introduced and discussed in Refs. [46,47]. It shows that birds could use the information of a whole group to find their directions. Hence, birds act as particles that would update their velocities and positions by the best experience of a whole group *gbest* and their own *pbest* during each flight (iteration). The number

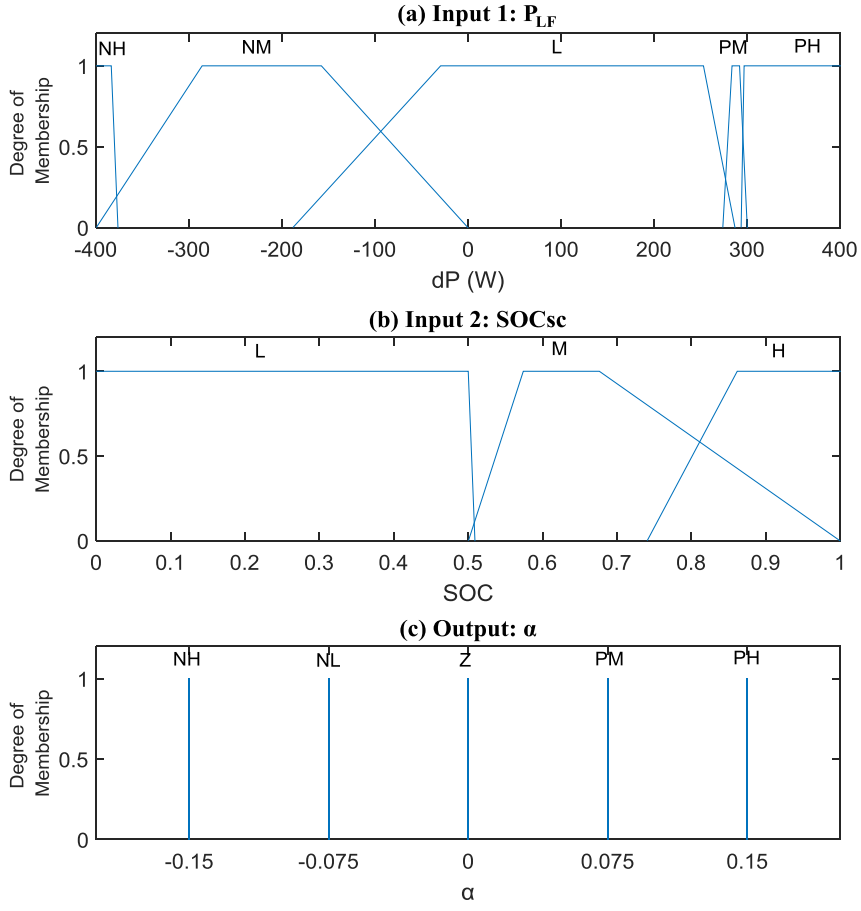

Fig. 4. Input and Output Membership Functions: (a) Input 1: P_{LF} (b) Input 2: SOCsc (c) Output: α.

of variables in each problem determines the dimension of the particles. The quality of solution for each particle is measured by a fitness function evaluated at the particle's current position.

Since the prediction of electrical load [37–39] and solar irradiance [34–36] are possible by using the machine learning algorithms, the FLC can be optimized based on the predicted data. In this study, the solar irradiation profile and load demand of a rural household as shown in Fig. 2(a) and (b) are assumed as the predicted data. The MFs of the input variables of FLC are optimized based on the predicted solar irradiation data and load demand. A complete trapezoidal MF is constructed by four points. For a variable with more than two trapezoidal MFs, each of the first (left) MF and the last (right) MF has only two points to be tuned. Therefore, the number of points optimized for a variable, n, can be calculated by using equation (9).

$$n = (4 \times mf) - 4 \tag{9}$$

where mf is the number of MF. In the proposed control strategy, the input variable P_{LF} and SOCsc have five and three MFs, respectively. As a result, a total of 24 points are needed to be optimized by the PSO algorithm. Hence, a FLC or solution can be represented by a particle with 24 dimensions. Fig. 5 presents the flowchart of the PSO procedure where the population size and the number of iteration are user-defined.

3.3.4. Fitness function

The high discharge current of the battery is extremely harmful to the battery as it increases the sludging rate of positive active mass and the temperature of the battery [48–50]. The main objective of the optimization is to minimize the battery peak current without discharging the SC below 50% of SOCsc. The battery peak current reduction is able to improve the battery efficiency and battery lifespan as well as to reduce the cost of the system [4,5,51]. In PSO, the fitness of the solution is evaluated by the fitness function, $f(x)$. In this study, the $f(x)$ is defined in equation (10) which is the maximum value of the battery current.

$$f(x) = \max(I_{batt}) \tag{10}$$

where I_{batt} is the battery current. In every iteration, the maximum battery current of each solution is recorded for PSO algorithm to search for the better solution.

4. Result and discussion

4.1. PSO optimization

The MFs of FLC are optimized by PSO based on the solar irradiation and load profiles as shown in Fig. 2(a) and (b). Fig. 5 illustrates the flowchart of PSO optimization, where a total of 80 iterations and the population size of 20 particles are defined. Each particle with 24 dimensions represents a FLC model. The fitness function, as introduced in equation (10), is used to evaluate the fitness of every particle in the population. The personal best of the particle, *pbest*, and global best, *gbest*, are updated after every evaluation.

Fig. 6 shows the graph of fitness value against the number of iteration. The *gbest* of the first iteration is 6.0332 A in which the solution is generated randomly. The fitness value decreases as the iteration increases. At 60th iteration, the *gbest* is reduced to 5.7116 A and maintained until the 80th iteration. By the end of the optimization process, the best solution (the particle with *gbest* of 5.7116 A) is transformed into a FLC model as illustrated in Fig. 4.

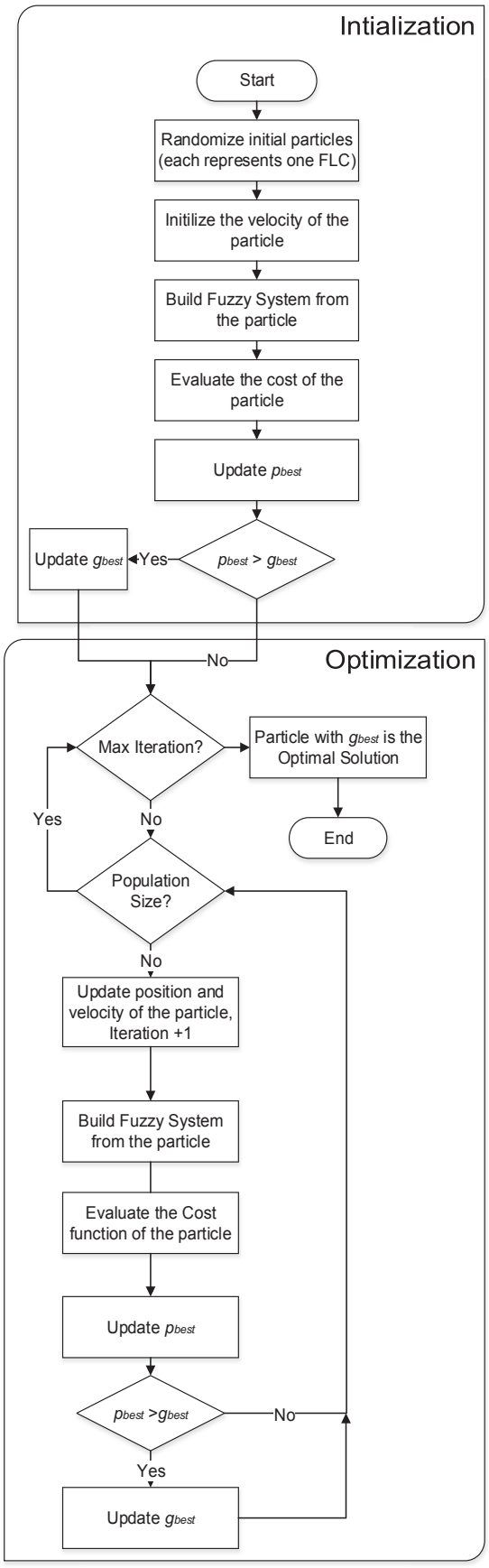

Fig. 5. Flowchart of optimization process.

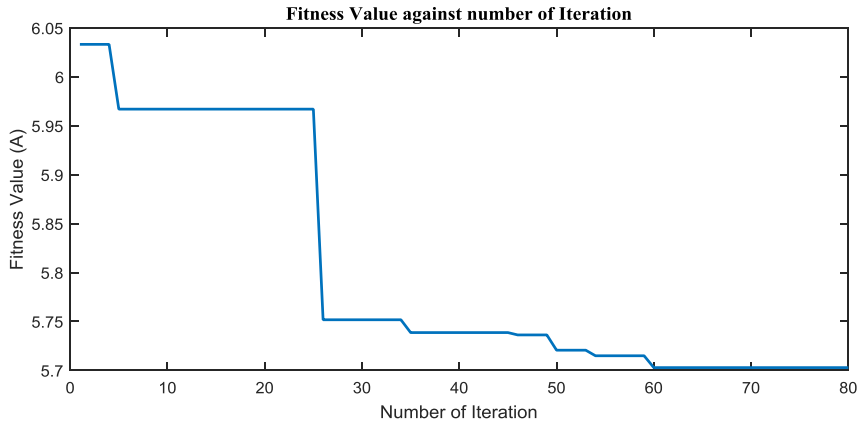

Fig. 6. Convergence curve of PSO algorithm for optimization in 80 iterations.

4.2. Simulation

In this study, four models as listed in Table 5 are constructed in Simulink. Model I is the conventional standalone PV system with battery-only system. Model II is the standalone PV system with Battery-Supercapacitor HESS with RBC. Model III is the standalone PV system with Battery-Supercapacitor HESS with HPF-based FBC. Lastly, Model IV is the standalone PV system with Battery-Supercapacitor HESS with the proposed control strategy. The configuration of the control strategies is illustrated in Table 5. The solar irradiation and the load profiles, as illustrated in Fig. 2(a) and (b), are modelled and applied for all the models.

Several battery parameters particularly battery peak current (I_{batt_peak}), battery peak power (P_{batt_peak}), average battery SOC ($SOC_{batt\_average}$), and final battery SOC (SOC_{batt_final}) are evaluated. The reduction of I_{batt_peak} and P_{batt_peak} would lead to lower battery stress, higher battery efficiency, and reduction of internal voltage in the battery [4,5]. The $SOC_{batt\_average}$ and SOC_{batt_final} are evaluated in this study in which higher $SOC_{batt\_average}$ and SOC_{batt_final} would extend the battery lifetime and reduce the LPSP of the system [23]. The $|\Delta P|$, in Watt per second (W s^{-1}), refers to the absolute value of the rate of change of power in time step of Δt. $|\Delta P|$ can be calculated by using equation (11).

$$|\Delta P| = \left|\frac{P(t) - P(t - \Delta t)}{\Delta t}\right| \tag{11}$$

where $P(t)$ is the battery power at the time t, $P(t\text{-}\Delta t)$ is the battery power at time $t\text{-}\Delta t$, and Δt is the time step which is 1 s in this study. In other words, $|\Delta P|$ can be used to determine the level of fluctuation of the battery power, where the higher the $|\Delta P|$, the higher the level of fluctuation. With low level of fluctuation in the battery power, the efficiency and life expectancy of the battery can be increased which in turn reducing the cost of the energy source [4]. The maximum of $|\Delta P|$ ($|\Delta P|_{max}$) and the mean of $|\Delta P|$ ($|\Delta P|_{mean}$) of the battery power are computed in this study to evaluate the battery dynamic stress level.

Fig. 7(a)–(d) show the battery power profile of all the models in the simulation. Table 6 summarizes and compares the battery performance of all the models. For Model I, the battery is the only energy storage system to satisfy the power mismatch between the PV output power and the load demand. As a result, the battery power profile as shown in Fig. 7(a) is identical to the profile of dP as shown in Fig. 2 (d). Hence, Models II, III, and IV are compared to the Model I to evaluate the performance of the control strategies.

For Model II, Fig. 7(b) and Table 6 summarize that the I_{batt_peak} and P_{batt_peak} are reduced but the battery still experiences highly fluctuating power demand. Table 6 shows that the $SOC_{batt\_average}$ and SOC_{batt_final} are improved by 0.63% and 1.32%, respectively which are the highest in all the models as the SC discharges most of its energy to supply the load. For Model III, Fig. 7(c) and Table 6 show that the dynamic stress level of the battery has a considerable reduction but the I_{batt_peak} and P_{batt_peak} are not improved significantly. This is because of the FBC that is designed to reduce the dynamic stress of the battery without considering the peak demand. On the other hand, the $SOC_{batt\_average}$ and SOC_{batt_final} are not improved substantially (~0%) as only the highly fluctuating low power components are absorbed by the SC.

For Model IV, it is evident that the battery power profile is smoother than Model I and II as shown in Fig. 7(d). The mismatch between dP and battery power is compensated by SC. Fig. 7(e)–(h) present the processing signals of P_{LF}, P_{HF}, P_H, and P_{SC} in the proposed control strategy. As illustrated in Fig. 3(c), the dP profile is being processed by the LPF. The P_{LF} as illustrated in Fig. 7(e) is the output of the LPF. By referring to equation (5), the P_{HF}, as shown in Fig. 7(f), is the mismatch between dP and P_{LF}. The P_{HF} is a highly fluctuating power demand which is desirable to be supplied by the SC. The P_H, as shown in Fig. 7(g), is determined by the PSO-optimized FLC to

Table 5
The Configuration of the models in simulink.

Model	Energy storage system	Control strategy	Parameters	
I	Battery	–	–	
II	Battery/SC	RBC	ib1	5.5
			ib2	−5.5
			K1	1
			K2	−1
III	Battery/SC	FBC	Passband Edge Frequency	0.001 rad/s
IV (Proposed System)	Battery/SC	Proposed Control Strategy	Passband Edge Frequency	0.002 rad/s
			Optimization	PSO

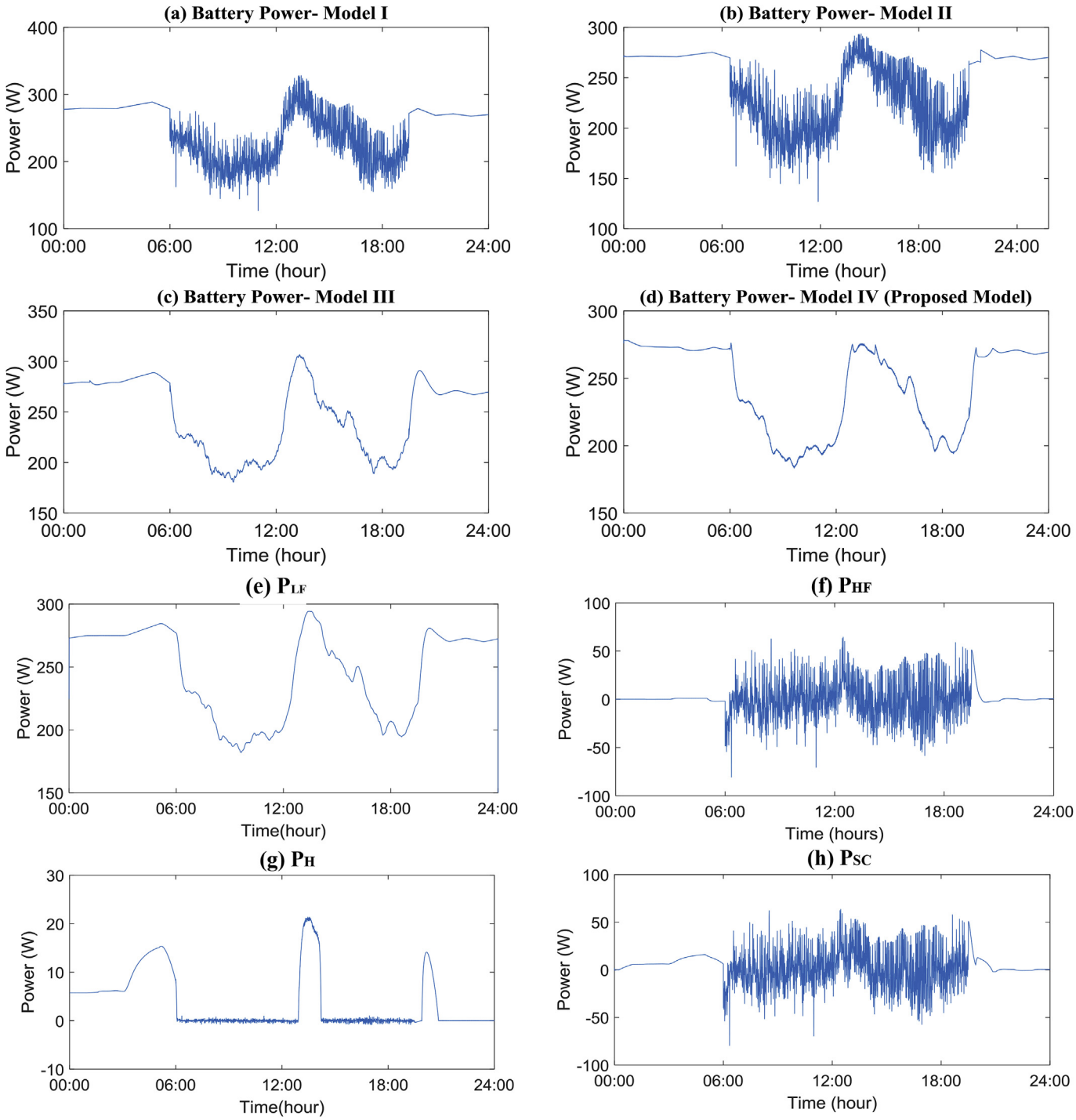

Fig. 7. Simulation results throughout the 24-h Simulink simulation: (a) Battery Power - Model I. (b) Battery Power - Model II. (c) Battery Power -Model III. (d) Battery Power -Model IV. (Proposed Model) (e) P_{LF} Processing Signal. (f) P_{HF} Processing Signal. (g) P_H Processing Signal. (h) P_{SC} Processing Signal.

reduce the battery peak demand. The P_{SC}, as shown in Fig. 7(h), is the combination of the profiles of P_{HF} and P_H as expressed in equation (7).

As mentioned previously, one of the objectives of the proposed control strategy is to reduce the peak demand of the battery. In the simulation, the maximum battery current in Model IV is 5.7116 A, which is identical to the *gbest* as the same solar irradiation and load profiles are used in the PSO optimization and simulation. Model IV has achieved the greatest improvement in terms of the reduction of I_{batt_peak}, P_{batt_peak}, $|\Delta P|_{max}$, and $|\Delta P|_{mean}$. With the presence of FLC in the proposed control strategy, the SC discharges appropriately to meet the peak demand by constantly considering the SOC level of SC. Hence, the I_{batt_peak} and P_{batt_peak} are reduced by 16.05% and 15.19%, respectively in comparison to Model I. Meanwhile, the $|\Delta P|_{max}$ and $|\Delta P|_{mean}$ of the battery is reduced by 77.01% and 95.65%, respectively with the implementation of LPF in the proposed strategy. The $SOC_{batt\_average}$ and SOC_{batt_final} are improved by 0.48% and 1.15%, respectively which is slightly lower than Model II as the

Table 6
Summary and Comparison of the Battery Performance of all the models.

Battery parameters		Model I	Model II	Model III	Model IV (Proposed system)
I_{batt_peak}	Current (A)	6.8038	6.082	6.1446	5.7116
	Reduction (%)	–	10.61	9.69	16.05
P_{batt_peak}	Power(W)	328.368	293.655	296.5788	278.4766
	Reduction (%)	–	10.57	9.68	15.19
$SOC_{batt\_average}$	SOC (%)	66.8786	67.3007	66.8475	67.2017
	Increment (%)	–	0.63	−0.05	0.48
SOC_{batt_final}	SOC (%)	47.3189	47.9457	47.3223	47.8638
	Increment (%)	–	1.32	0.01	1.15
$\|\Delta P\|_{max}$	Rate (W s^{-1})	32.6814	24.0930	8.4636	7.5144
	Reduction (%)	–	26.28	74.15	77.01
$\|\Delta P\|_{mean}$	Rate (W s^{-1})	0.37778	0.338	0.01886	0.01666
	Reduction (%)	–	10.33	95.01	95.59

SC discharges most of its energy to fulfil the objectives of the control strategy.

The level of SC utilization in the HESS can be determined by calculating the absolute value of the accumulated ampere-hours (amount of charge) going to and from the SC, $|Ah|_{SC}$. The SC ampere-hours are calculated by integrating the SC current over time. Fig. 8(a) and Fig. 8(b) illustrate the SOCsc and $|Ah|_{SC}$ of Models II, III, and IV throughout the simulation. The higher the level of SC utilization, the lower the level of battery utilization. As a result, the internal losses of the system can be reduced by increasing the level of SC utilization. This is due to a large part of the output current flowing through the SC which has a smaller internal resistance, and thus leading to a lower heating of the battery as well as a longer battery lifespan [6].

Fig. 8(b) depicts that the final SOCsc of Model II is equal to the minimum SOCsc of 50%. Model II does not utilize the SC effectively as it not only consumes most of the SC energy but also achieves the worst performance in terms of SC utilization and battery dynamic stress reduction compared to other models with HESS. Subsequently, the total $|Ah|_{SC}$ of Model III is 487.86% higher than Model II but 32.65% lower than Model IV. The final SOCsc of Model III is 92.69%, where only 0.56% net SOCsc is utilized throughout the simulation. In other words, the SC of Model III is underutilized. For Model IV, the final SOCsc is maintained at a higher level as compared to Model II while maintaining the SOCsc by 7.45% above the minimum SOC of 50%. The total $|Ah|_{SC}$ of Model IV is the highest in comparison to the other models, where the level of SC utilization is 687.122% and 32.65% higher than Model II and Model III,

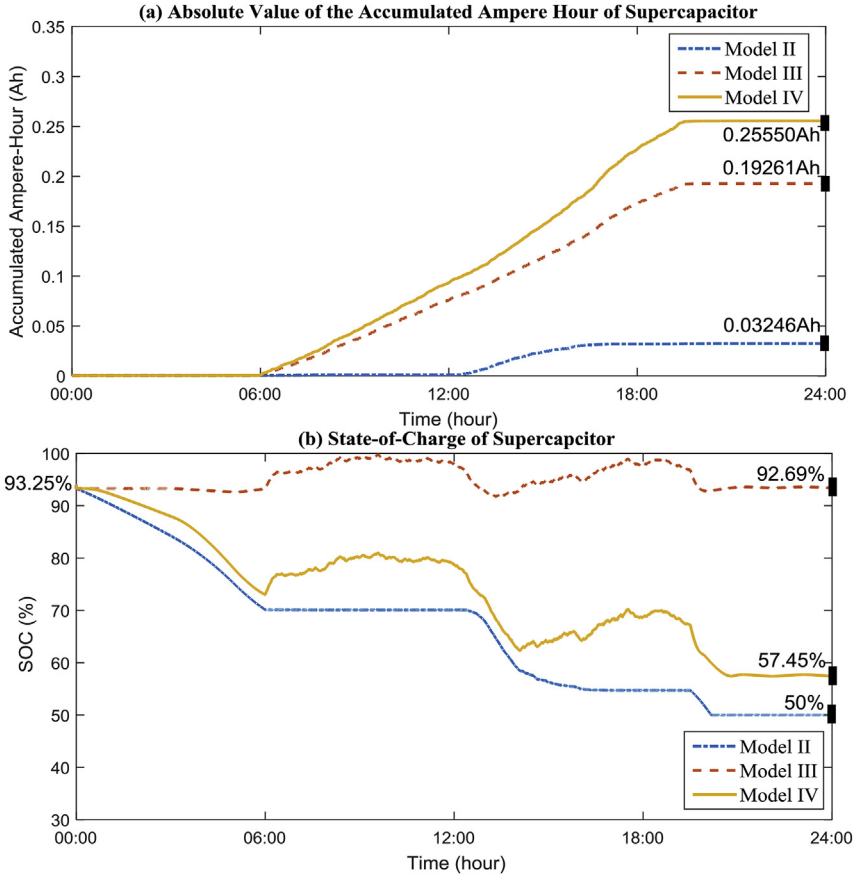

Fig. 8. Performance of Supercapacitor throughout the 24-h Simulink simulation.

respectively. In short, the proposed strategy is able to operate the SC within the recommended SOC range and utilize the limited energy capacity of SC effectively to achieve an excellent performance.

The proposed system (Model IV) is tested with different weather profiles where higher solar irradiation levels and the load profile as shown in Fig. 2(b) are used. As expected, the reduction of battery peak demand and battery dynamic stress level are the most significant in the scenario with low level solar irradiation profile (29th Dec 2014) as higher stress level is imposed to the Battery-Supercapacitor HESS. The simulation results show that proposed system reduces the battery dynamic stress ($|\Delta P|_{mean}$) significantly by more than 80% in comparison to Model I regardless of the solar irradiation profile. Meanwhile, the reduction of battery peak demand is depending on the stress level of dP which is determined by the solar irradiation level and the load demand. The battery peak demand reduction can be significant when there is a high dP demand due to the low PV output or peak load demand.

5. Conclusion

In this study, the Simulink model of the proposed standalone PV system with Battery-Supercapacitor HESS and an optimal control strategy are presented. The objectives of the proposed system are to reduce the dynamic stress and peak power demand of the battery by employing LPF and FLC. PSO algorithm is implemented to tune the MFs of the FLC in order to optimize the battery peak current reduction. The proposed system is evaluated and compared to the conventional system with battery-only systems and the systems with conventional control strategies (RBC and FBC). The simulation results show that the dynamic stress and peak current demand of the battery in the proposed system are greatly improved, which will eventually extend the battery lifespan. The proposed system is able to operate the SC within the recommended SOC range and utilize the limited energy of SC effectively to perform better than the conventional systems.

References

[1] A.Q. Jakhrani, A.-K. Othman, A.R.H. Rigit, S.R. Samo, Life cycle cost analysis of a standalone PV system, in: 2012 Int. Conf. Green Ubiquitous Technol, IEEE, Jakarta, Indonesia, 2012, pp. 82–85, http://dx.doi.org/10.1109/GUT.2012.6344195.

[2] S.Y. Kan, M. Verwaal, H. Broekhuizen, The use of battery-capacitor combinations in photovoltaic powered products, J. Power Sources 162 (2006) 971–974, http://dx.doi.org/10.1016/j.jpowsour.2005.07.001.

[3] J. Schiffer, D.U. Sauer, H. Bindner, T. Cronin, P. Lundsager, R. Kaiser, Model prediction for ranking lead-acid batteries according to expected lifetime in renewable energy systems and autonomous power-supply systems, J. Power Sources 168 (2007) 66–78, http://dx.doi.org/10.1016/j.jpowsour.2006.11.092.

[4] A.C. Baisden, A. Emadi, ADVISOR-based model of a battery and an ultracapacitor energy source for hybrid electric vehicles, IEEE Trans. Veh. Technol. 53 (2004) 199–205, http://dx.doi.org/10.1109/TVT.2003.822004.

[5] R.A. Dougal, S. Liu, R.E. White, Power and life extension of battery-ultracapacitor hybrids, IEEE Trans. Components Packag. Technol. 25 (2002) 120–131, http://dx.doi.org/10.1109/6144.991184.

[6] S. Pay, Y. Baghzouz, Effectiveness of battery-supercapacitor combination in electric vehicles, in: 2003 IEEE Bol. PowerTech - Conf. Proc, 2003, pp. 728–733, http://dx.doi.org/10.1109/PTC.2003.1304472.

[7] Y. Zhu, F. Zhuo, H. Shi, Power management Strategy research for a photovoltaic-Hybrid Energy Storage System, in: ECCE Asia Downunder (ECCE Asia), IEEE, Melbourne, VIC, 2013, pp. 842–848, http://dx.doi.org/10.1109/ECCE-Asia.2013.6579202.

[8] G. Wang, M. Ciobotaru, V.G. Agelidis, Power smoothing of large solar PV plant using hybrid energy storage, IEEE Trans. Sustain. Energy 5 (2014) 834–842, http://dx.doi.org/10.1109/TSTE.2014.2305433.

[9] T.-L. Pan, H.-S. Wan, Z.-C. Ji, Stand-alone wind power system with battery/supercapacitor hybrid energy storage, Int. J. Sustain. Eng. 7 (2014) 103–110, http://dx.doi.org/10.1080/19397038.2013.779327.

[10] S.K. Kollimalla, M.K. Mishra, N.N. Lakshmi, Coordinated control and energy management of hybrid energy storage system in PV system, in: 2014 Int. Conf. Comput. Power, Energy, Inf. Commun. ICCPEIC 2014, 2014, pp. 363–368, http://dx.doi.org/10.1109/ICCPEIC.2014.6915391.

[11] M.E. Glavin, P.K.W. Chan, S. Armstrong, W.G. Hurley, A stand-alone photovoltaic supercapacitor battery hybrid energy storage system, in: 2008 13th Int. Power Electron. Motion Control Conf. EPE-PEMC 2008, 2008, pp. 1688–1695, http://dx.doi.org/10.1109/EPEPEMC.2008.4635510.

[12] Y.Y. Chia, L.H. Lee, N. Shafiabady, D. Isa, A load predictive energy management system for supercapacitor-battery hybrid energy storage system in solar application using the Support Vector Machine, Appl. Energy 137 (2015) 588–602, http://dx.doi.org/10.1016/j.apenergy.2014.09.026.

[13] Y.D. Song, Q. Cao, X. Du, H.R. Karimi, Control strategy based on wavelet transform and neural network for hybrid power system, J. Appl. Math. 2013 (2013) 1–8, http://dx.doi.org/10.1155/2013/375840.

[14] N. Mendis, K.M. Muttaqi, S. Perera, Active power management of a super capacitor-battery hybrid energy storage system for standalone operation of DFIG based wind turbines, in: 2012 IEEE Ind. Appl. Soc. Annu. Meet, 2012, pp. 1–8, http://dx.doi.org/10.1109/IAS.2012.6374045.

[15] A.M. Gee, F.V.P. Robinson, R.W. Dunn, Analysis of battery lifetime extension in a small-scale wind-energy system using supercapacitors, IEEE Trans. Energy Convers. 28 (2013) 24–33, http://dx.doi.org/10.1109/TEC.2012.2228195.

[16] S.K. Kollimalla, M.K. Mishra, N.L. Narasamma, Design and analysis of novel control strategy for Battery and Supercapacitor Storage System, IEEE Trans. Sustain. Energy 5 (2014) 1137–1144, http://dx.doi.org/10.1109/TSTE.2014.2336896.

[17] T. Kim, H. Moon, D. Kwon, S. Moon, A Smoothing Method for Wind Power Fluctuation Using Hybrid Energy Storage, 2015, pp. 1–6.

[18] N.R. Tummuru, M.K. Mishra, S. Srinivas, Dynamic Energy management of Hybrid Energy Storage System with High-gain PV converter, IEEE Trans. Energy Convers. 30 (2015) 150–160, http://dx.doi.org/10.1109/TEC.2014.2357076.

[19] A.M. Osman Haruni, M. Negnevitsky, M.E. Haque, A. Gargoom, A novel operation and control strategy for a standalone hybrid renewable power system, IEEE Trans. Sustain. Energy 4 (2013) 402–413, http://dx.doi.org/10.1109/TSTE.2012.2225455.

[20] P. García, C.A. García, L.M. Fernández, F. Llorens, F. Jurado, ANFIS-Based control of a grid-connected hybrid system integrating renewable energies, hydrogen and batteries, IEEE Trans. Ind. Inf. 10 (2014) 1107–1117, http://dx.doi.org/10.1109/TII.2013.2290069.

[21] P. García, J.P. Torreglosa, L.M. Fernández, F. Jurado, Optimal energy management system for stand-alone wind turbine/photovoltaic/hydrogen/battery hybrid system with supervisory control based on fuzzy logic, Int. J. Hydrogen Energy 38 (2013) 14146–14158, http://dx.doi.org/10.1016/j.ijhydene.2013.08.106.

[22] J. Li, Y. Liu, S. Wang, J. Shi, L. Ren, K. Gong, Y. Tang, Design and advanced control strategies of a hybrid energy storage system for the grid integration of wind power generations, IET Renew. Power Gener. 9 (2015) 89–98, http://dx.doi.org/10.1049/iet-rpg.2013.0340.

[23] M. Sarvi, I.N. Avanaki, An optimized fuzzy logic controller by water cycle algorithm for power management of stand-alone Hybrid green power generation, Energy Convers. Manag. 106 (2015) 118–126, http://dx.doi.org/10.1016/j.enconman.2015.09.021.

[24] R. Yumurtaci, Role of energy management in hybrid renewable energy systems: case study based analysis considering varying seasonal conditions, Turk. J. Electr. Eng. Comput. Sci. 21 (2013) 1077–1091, http://dx.doi.org/10.3906/elk-1112-85.

[25] P. Dash, M.H. Athari, M.M. Ardehali, Operational performance of energy storage as function of electricity prices for on-grid hybrid renewable energy system by optimized fuzzy logic controller, Renew. Energy 85 (2016) 890–902, http://dx.doi.org/10.1016/j.renene.2015.07.055.

[26] S. Safari, M.M. Ardehali, M.J. Sirizi, Particle swarm optimization based fuzzy logic controller for autonomous green power energy system with hydrogen storage, Energy Convers. Manag. 65 (2013) 41–49, http://dx.doi.org/10.1016/j.enconman.2012.08.012.

[27] R. Cozzolino, L. Tribioli, G. Bella, Power management of a hybrid renewable system for artificial islands: a case study, Energy 106 (2016) 774–789, http://dx.doi.org/10.1016/j.energy.2015.12.118.

[28] V. Dash, P. Bajpai, Power management control strategy for a stand-alone solar photovoltaic-fuel cell–battery hybrid system, Sustain. Energy Technol. Assessments 9 (2015) 68–80, http://dx.doi.org/10.1016/j.seta.2014.10.001.

[29] P. García, J.P. Torreglosa, L.M. Fernández, F. Jurado, Improving long-term operation of power sources in off-grid hybrid systems based on renewable energy, hydrogen and battery, J. Power Sources 265 (2014) 149–159. http://dx.doi.org/10.1016/j.jpowsour.2014.04.118.

[30] A. Brka, G. Kothapalli, Y.M. Al-Abdeli, Predictive power management strategies for stand-alone hydrogen systems: lab-scale validation, Int. J. Hydrogen Energy 40 (2015) 9907–9916, http://dx.doi.org/10.1016/j.ijhydene.2015.06.081.

[31] Z. Song, H. Hofmann, J. Li, J. Hou, X. Han, M. Ouyang, Energy management strategies comparison for electric vehicles with hybrid energy storage system, Appl. Energy 134 (2014) 321–331, http://dx.doi.org/10.1016/j.apenergy.2014.08.035.

[32] N. Altin, I. Sefa, dSPACE based adaptive neuro-fuzzy controller of grid interactive inverter, Energy Convers. Manag. 56 (2012) 130–139, http://dx.doi.org/10.1016/j.enconman.2011.11.017.

[33] A.T. Azar, in: Fuzzy Systems, first ed., InTech, Vukovar, Crotia, 2010 http://dx.doi.org/10.5772/56527.

[34] A. Mellit, A.M. Pavan, A 24-h forecast of solar irradiance using artificial neural

network: application for performance prediction of a grid-connected PV plant at Trieste, Italy, Sol. Energy 84 (2010) 807–821, http://dx.doi.org/10.1016/j.solener.2010.02.006.
[35] Y. El Mghouchi, T. Ajzoul, A. El Bouardi, Prediction of daily solar radiation intensity by day of the year in twenty-four cities of Morocco, Renew. Sustain. Energy Rev. 53 (2016) 823–831, http://dx.doi.org/10.1016/j.rser.2015.09.059.
[36] Y. El Mghouchi, T. Ajzoul, D. Taoukil, A. El Bouardi, The most suitable prediction model of the solar intensity, on horizontal plane, at various weather conditions in a specified location in Morocco, Renew. Sustain. Energy Rev. 54 (2016) 84–98, http://dx.doi.org/10.1016/j.rser.2015.09.089.
[37] K. Lee, Y. Cha, J. Park, Short-term load forecasting using an artificial neural network, Power Syst. IEEE Trans. 7 (1992) 124–132. http://ieeexplore.ieee.org/xpls/abs_all.jsp?arnumber=141695.
[38] Thesis Submitted In Partial Fulfillment Of The Requirements For The Degree Of Bachelor Of Technology M. Kumar, Short-Term load forecasting using artificial neural network techniques load forecasting using artificial neural network, Electr. Eng. (2009) 25–38.
[39] D.C. Park, M.A. El-Sharkawi, R.J. Marks, L.E. Atlas, M.J. Damborg, Electric load forecasting using an artificial neural network, IEEE Trans. Power Syst. 6 (1991) 442–449, http://dx.doi.org/10.1109/59.76685.
[40] L.W. Chong, Y.W. Wong, R.K. Rajkumar, R.K. Rajkumar, D. Isa, Hybrid energy storage systems and control strategies for stand-alone renewable energy power systems, Renew. Sustain. Energy Rev. 66 (2016) 174–189. http://dx.doi.org/10.1016/j.rser.2016.07.059.
[41] I. MathWorks, Comparison of Sugeno and Mamdani Systems, http://www.mathworks.com/help/fuzzy/comparison-of-sugeno-and-mamdani-systems.html, 2016 (accessed April 3, 2016).
[42] M. Ali Akcayol, Application of adaptive neuro-fuzzy controller for SRM, Adv. Eng. Softw. 35 (2004) 129–137, http://dx.doi.org/10.1016/j.advengsoft.2004.03.005.
[43] F. Garcia-Torres, C. Bordons, Optimal economical schedule of hydrogen-based microgrids with hybrid storage using model predictive control, IEEE Trans. Ind. Electron. 62 (2015) 5195–5207, http://dx.doi.org/10.1109/TIE.2015.2412524.
[44] A. Kuperman, I. Aharon, Battery-ultracapacitor hybrids for pulsed current loads: a review, Renew. Sustain. Energy Rev. 15 (2011) 981–992, http://dx.doi.org/10.1016/j.rser.2010.11.010.
[45] Y.Z.Y. Zhang, Z.J.Z. Jiang, X.Y.X. Yu, Control strategies for Battery/Supercapacitor Hybrid Energy Storage Systems, in: 2008 IEEE Energy 2030 Conf, 2008, pp. 5–10, http://dx.doi.org/10.1109/ENERGY.2008.4781031.
[46] R. Poli, J. Kennedy, T. Blackwell, Particle swarm optimization, Swarm Intell. 1 (2007) 33–57, http://dx.doi.org/10.1007/s11721-007-0002-0.
[47] J. Kennedy, R. Eberhart, Particle swarm optimization, neural networks, 1995, in: Proceedings., IEEE Int. Conf vol. 4, 1995, pp. 1942–1948, http://dx.doi.org/10.1109/ICNN.1995.488968.
[48] N. Omar, J. Van Mierlo, B. Verbrugge, P. Van den Bossche, Power and life enhancement of battery-electrical double layer capacitor for hybrid electric and charge-depleting plug-in vehicle applications, Electrochim. Acta 55 (2010) 7524–7531. http://dx.doi.org/10.1016/j.electacta.2010.03.039.
[49] P. Lailler, F. Zaninotto, S. Nivet, L. Torcheux, J.-F. Sarrau, J.-P. Vaurijoux, D. Devilliers, Study of the softening of the positive active-mass in valve-regulated lead-acid batteries for electric-vehicle applications, J. Power Sources 78 (1999) 204–213. http://dx.doi.org/10.1016/S0378-7753(99)00038-5.
[50] P. Ruetschi, Aging mechanisms and service life of lead–acid batteries, J. Power Sources 127 (2004) 33–44. http://dx.doi.org/10.1016/j.jpowsour.2003.09.052.
[51] G. Papazov, D. Pavlov, Influence of cycling current and power profiles on the cycle life of lead/acid batteries, J. Power Sources 62 (1996) 193–199. http://dx.doi.org/10.1016/S0378-7753(96)02422-6.